Construction and Building Materials 146 (2017) 775–787

Contents lists available at ScienceDirect

Construction and Building Materials

journal homepage: www.elsevier.com/locate/conbuildmat

Recognition, location, measurement, and 3D reconstruction of concealed cracks using convolutional neural networks

Zheng Tong [a,b], Jie Gao [a,c], Haitao Zhang [b,*]

[a] School of Highway, Chang'an University, Xi'an 710061, China
[b] College of Civil Engineering, Northeast Forestry University, Harbin 150040, China
[c] National and Local Joint Engineering Materials Laboratory of Traffic and Civil Engineering, Chongqing Jiaotong University, Chongqing 400074, China

HIGHLIGHTS

- Project presents an application of convolutional neural networks (CNN) in cracks.
- Different CNNs are established by the processes of structure design, training and testing.
- The crack feature points are extracted by feature extraction CNN to establish 3D model.
- CNN is able to recognize concealed cracks from other damage in GPR images with zero error.
- CNNs could be accurately used for the recognition, location of concealed crack of asphalt pavement.

ARTICLE INFO

Article history:
Received 1 December 2016
Received in revised form 26 March 2017
Accepted 12 April 2017

Keywords:
Asphalt pavement
Concealed cracks
Convolutional neural networks (CNNs)
Ground penetrating radar (GPR)
Image measurement

ABSTRACT

Concealed cracks in asphalt pavement are the cracks that originate below the surface of the pavement. These cracks are a major contributing factor to pavement damage, in addition to being a major contributing factor to the formation of reflection cracks. The detection of a concealed crack is considered challenging because the location of the crack is, by definition, difficult to find. Therefore, the research on the utilization of ground penetrating radar (GPR) to locate concealed cracks has gained significant interest in recent years. However, the manually processed GPR image used for the recognition, location, and measurement of concealed cracks is inefficient and inaccurate. This project presents an application of convolutional neural networks (CNNs) to GPR images that automatically recognizes, locates, measures, and produces a 3D reconstruction of concealed cracks. In this project, three different CNNs (recognition, location, and feature extraction) were established to accomplish the aforementioned tasks automatically. Each CNN is developed through processes of structural design, training, and testing. The recognition CNN was designed to distinguish concealed cracks from other types of damage in a GPR image, the location CNN determined the location and length measurement of concealed crack images based on the results provided by the recognition CNN, and crack feature points were extracted by the feature extraction CNN to establish the 3D reconstruction models of the concealed cracks. The 3D reconstruction models were then used to calculate crack volume and predict the growth tendency of cracks. The results indicated that the recognition CNN is able to distinguish concealed cracks from other types of damages in 6482 GPR images with zero errors. In addition, the length recognition results calculated from the location CNN possess a 0.2543 cm mean squared error, a 0.978 cm maximum length error, and a 0.504 cm average error in the test samples. Meanwhile, the feature extraction CNN is able to provide feature points for a 3D reconstruction model. The results of this study suggest that the CNNs could be accurately used for the recognition, location, and 3D reconstruction of concealed cracks in asphalt pavement in real-world applications.

1. Introduction

The semi-rigid base in an asphalt pavement structure is the most popular structure in Chinese highways because of its two main advantages: low investment cost and straightforward manufacturing process. Therefore, more than 950,000 km of highway were

* Corresponding author.
E-mail address: zht6781@163.com (H. Zhang).

http://dx.doi.org/10.1016/j.conbuildmat.2017.04.097
0950-0618/

built using semi-rigid base in China until 2015, which perfectly meets the status of China's economic capability, which is that of a developing country. After decades of operation, a consensus has been reached in China, that the cracking of semi-rigid base structures is inevitable. Reflection cracks are the most common cracks in semi-rigid bases in China, and they always occur in either the semi-rigid base itself or in sub-bases before propagating to the surface. The formation of these cracks is the result of dry environments and temperature decrease in the semi-rigid bases and sub-bases. Reflection cracks can be visually observed, unlike concealed cracks. To prevent highway reflection cracks, it is necessary to detect them before they propagate to the surface. The cracks that occur in semi-rigid bases or sub-bases but have not yet transitioned into reflection cracks are called concealed cracks. Therefore, concealed cracks are the intermediate states of reflection cracks. If effective measures are taken to detect concealed cracks early, the formation of reflection cracks may be prevented. However, the detection of concealed cracks has proved to be very challenging, mostly because of their location below the pavement.

Ground penetrating radars (GPRs) have advantages such as high efficiency, safe operation, nondestructive operation, and high anti-interference [1–4], and therefore, are widely used in highway detection. In recent years, significant progress has been made in the utilization of GPRs for detecting concealed cracks in semi-rigid base and sub-base structures. However, there are several obvious disadvantages to this technology; namely, its dependency on other auxiliary instruments for damage recognition, complicated data preprocessing requirements, the difficulty in location automatically, and complicated 3D reconstruction operations [5–9]. Solla et al. [5] used GPR images to detect concealed cracks and successfully extracted their geometric features, but this method requires the assistance of infrared thermometers. In addition, Lu et al. [6] completed the recognition and location of concealed cracks in asphalt pavements, but the data preprocessing required to do so is complex. Xu et al. [7] successfully detected voids and cracks under the pavement using GPR, while the processes of category, location, and feature extraction of different types of damage all rely on artificial. Gracia et al. [8] analyzed GPR reflected waves to extract information on damage characteristics. Because different cracks have different specificities, the analysis workload is significant. Szymczyk et al. [9] used an S-transformation to successfully develop a three-dimensional reconstruction of GPR signals by using a complex conversion process. Obviously, these methods may not be able to automatically detect concealed cracks efficiently for their complex manual processes. Therefore, concealed crack detection should focus on the development of an automatic damage analysis system in GPR. The combination of GPR images and CNN may provide a potentially novel method for concealed crack detection.

The convolutional neural network (CNN) has advantages in the field of image recognition [10–13]. The CNN can be considered a type of highly nonlinear mapping that outputs the target features in a specified form based on the input image. The CNN is a type of artificial neural network whose structure of shared weights reduces the complexity of the network models, and the structure is similar to that of biological neural networks [14,15]. Images are used as the input data, which directly avoids the complex traditional recognition algorithm used in feature extraction and data reconstruction. The network structure has high invariance in the transformation of translation, scaling, tilting, and so on. This property can be used to analyze the complex shape changes of pavement cracks or voids [16–18]. Therefore, the introduction of CNN to the field of the concealed crack detection, combined with the use of GPR images instead of manual measurements, significantly improves the accuracy of the detection results and the efficiency of the detection processes. This is achieved without the use of high-performance hardware and personnel requirement, thereby reducing the associated costs.

In this research, attempts have been made to employ CNN to provide appropriate models for the automatic recognition, location, length measurement, and 3D reconstruction of concealed cracks in batches using GPR images of asphalt pavements. The technical outline of this study is organized as shown in Fig. 1. The preparation section presents the acquisition method of the GPR damage images. The experimental section details features of the proposed method, including the recognition CNN, the location and length CNN, and the feature extraction CNN. Then, the experimental results and discussions are presented.

2. Acquisition and preprocessing of GPR images

2.1. Collection device and method

A high-quality GPR image of a concealed crack is required to establish CNN models. However, the image quality is often influenced by the acquisition equipment and pavement structure. Therefore, the antenna type and frequency used should be selected according to the pavement structure to be examined. In this study, a LTD-2000 GPR (made in China) was adopted to capture images. The parameters of the LTD-2000 GPR include a 500 MHz shielding antenna (size: 30 cm × 30 cm × 14 cm), and a 20 cm transmitting-receiving antenna distance. The vertical and horizontal resolution ranges of the 500 MHz antenna were 0.15–0.27 cm and 3.0–5.2 cm, respectively, which were slightly influenced by the dielectric constants of the highway materials. The vertical resolution of the 500 MHz antenna could meet the engineering demands [19], but the horizontal resolution could not. Therefore, the widths of the concealed cracks could not be correctly reflected in the GPR images, and a revision should be made to calculate the actual values of the crack widths in the follow-up work for feature extraction.

The GPR image collection method also has an effect on image quality, especially the sharpness. The optimal collection method should utilize a reasonable detection point distance in order to guarantee high-quality images of damage. Therefore, the distances between checkpoints should be chosen based on the geometric features of the highway damage. Generally, the width of a concealed crack is less than 8 mm [20–22]. Based on the research of Lu et al. [6], a concealed crack can be detected by at least four echo signal records. Therefore, the checkpoint distances were selected to be 4 cm (L/5) apart in this research. A 4 cm (L/5) distance can guarantee that the GPR scans and records more than four echo signals from topmost point of the crack The scanning and recording of one echo signal is shown in Fig. 2. The antenna is activated to record an abnormal crack signal as its position is moved from location 1 to location 2. The distance between locations 1 and 2 was L/5. One effective concealed crack image included the four previously mentioned records. Then, denoising, wavelet analysis, and the detection results of GPR images were performed automatically by LTD-2000 systems based on the collected GPR data. Considering the influence of electromagnetic wave scattering and the origination point of the concealed cracks in the sub-bases, only the ranges from sub-bases to upper layers remained in the GPR images. This meets the requirements for highway detection [19]. In this method, the influence of all types of damage described previously were shown in the GPR images. The core sampling method shown in Fig. 3 was used to determine the types of disasters that occurred after GPR scanning.

2.2. GPR datasets

A typical GPR image of a concealed crack gathered using the above method is shown in Fig. 4a. The shape of the concealed crack

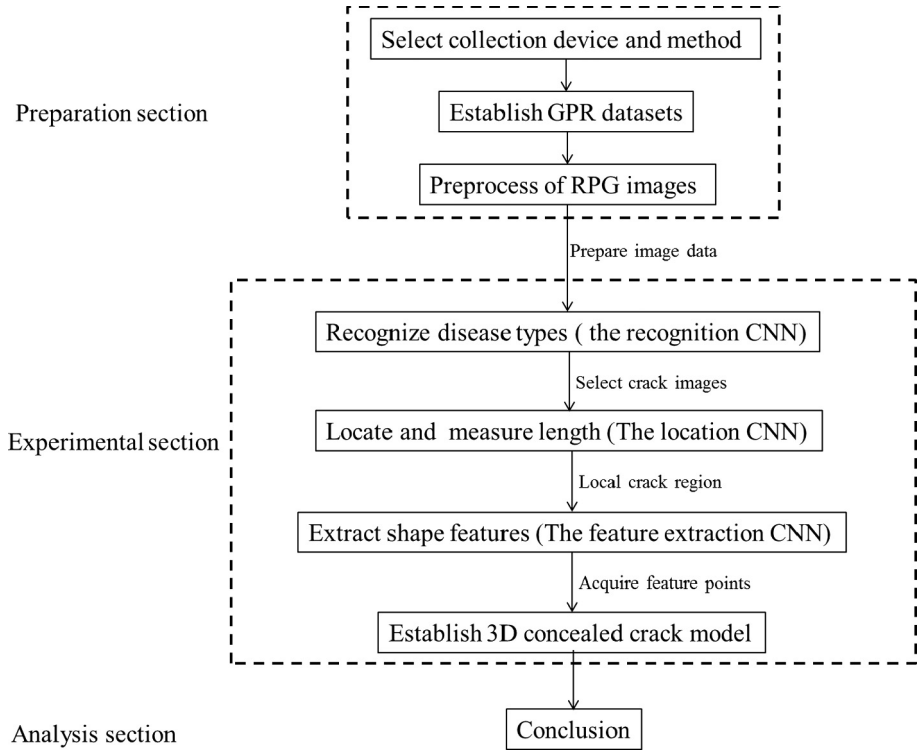

Fig. 1. Preprocess GPR images.

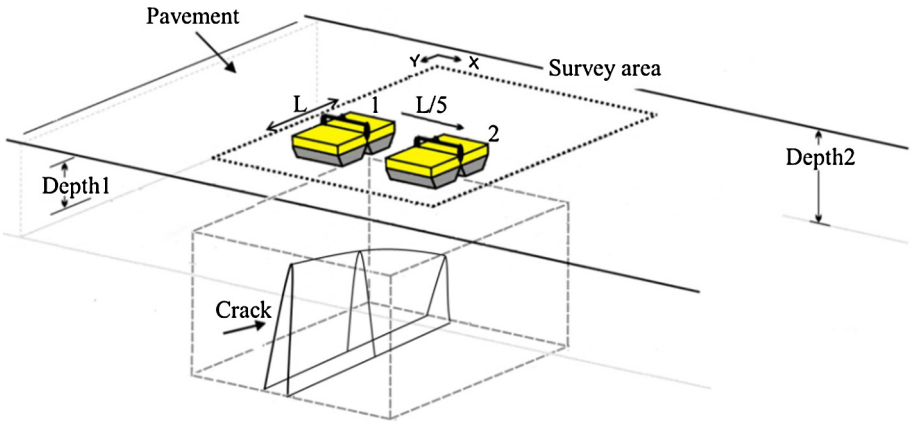

Fig. 2. One echo signal scanning and recording.

(a) Facilities for sampling core (b) Core with a concealed crack (c) Pavement damage after coring

Fig. 3. Core sampling method.

is a scattered hyperbola with symmetrical left and right sides. Typical GPR images of subgrade settlements and cavities in the roadbed are shown in Fig. 4b and c, respectively. The quantity of different types of damage shown in different images is listed in Table 1, the features of different highway structures are listed in Table 2, and the relative dielectric constants of different highway materials are listed in Table 3.

The color information in the images increased the difficulty of feature detection and recognition. Regarding the condition of algorithm difficulty, the color information was removed and images were saved as grey-scale maps.

Five hundred grey-scale maps were divided into 256×256 sized pixel images to be equal to the size of the CNN input layers. In addition, 6832 images with damage were acquired as the dataset of the CNN. Then, 2200 divided images, including 1000 divided images of concealed cracks, 500 divided images of subgrade settlement, 500 divided images of cavities in the roadbed, and 200 divided images without damage were selected from the dataset as the training samples for the CNNs. To ensure the integrity of the sample, all crack lengths should be included in the training samples. The rest of the 6832 images were used as testing samples.

3. Convolutional neural networks

A CNN is a type of deep neural network structure. Lecun et al. introduced this structure and utilized it in the image recognition field. Now, CNNs are mainly used to recognize 2D and 3D images [23,24]. The CNN has high robustness in order to overcome the transformation of translation, tilt, and displacement of an object [25,13]. This property was used to overcome the problems associated with structuring diseases that had irregular sizes and outlines Three CNNs with different functions were designed to perform automatic recognition, location, length measurement, and 3D reconstruction of concealed cracks in batches using GPR images. The process of developing one CNN is shown in Fig. 5. The process mainly involves the structure, training, and testing of of CNN. If the result of testing cannot satisfy the demand [19], the CNN should be re-structured and re-trained. The processes were realized based on Caffe, using a computer equipped with an Inter(R) Core(TM) i7-6700 CPU, 8.00 GB RAM, and NVIDIA GeForce GTX 1060 6GB GPU.

3.1. The recognition CNN

3.1.1. Design approach for the recognition CNN

The development of the recognition CNN includes the following steps:

(a) Preparation of training samples and test samples

As shown in similar studies on number classification and image classification [10,26,27], the typical sizes of a training sample and testing sample for recognition were approximately 100–1000 images for each object. Values within this range of typical sizes were used in our research on recognition. The dataset mentioned above was generated using 2200 images. This set of images included 1000 images of concealed cracks, 500 images of subgrade settlement, 500 images of roadbed cavities, and 200 images without damage. This dataset was randomly selected from the 6842 images mentioned in the preparation section, and was used as a training sample. The types of damages corresponding to these 2200 images were the target sample and were quadrature encoded as concealed crack $[1\ 0\ 0\ 0]'$, subgrade settlement$[0\ 1\ 0\ 0]'$, cavities $[0\ 0\ 1\ 0]'$, and no damage$[0\ 0\ 0\ 1]'$.. The rest of the 6832 images were used as testing samples to test the damage recognition capability of the recognition CNN.

(b) CNN structure

The structural design step aimed to confirm the basic structure of the CNN. The damage recognition CNN was composed of two convolutional layers (C1 and C2) and two subsampling layers (S1 and S2), followed by two full connection layers (F1 and F2) and the output layer. The details of the CNN are shown in Fig. 6. The size of input layer was 256×256. Because the size of input layer was equal to the size of the images, the input layer was selected based on two principles. First, the size of images should include an entire crack at least. Second, the sizes of the images should not be too large, in order to avoid dramatically increasing the computation load. Similar CNNs for number classification and image classification as shown in Refs. [10,26,27] were referred, and contained images sizes that were approximately in the ranges of 32×32 to 300×300. Considering these two conditions and similar CNNs for classification, 256×256 was selected as the image size for recognition. The function of C1 and C2 was to extract image features. The images were executed convolutions and reappeared as feature matrixes based on the activation function sigmoid after they were inputted C1 or C2 layer. The activation function sigmoid is shown in formula (1). Because C1 and C2 consisted of 6 and 14 convolution kernels respectively, and each convolution kernel has different weights and biases, different feature matrixes were acquired. Then, the function of S1 and S2 was to create aggregate statistics based on different feature matrixes to avoid excessive useless information being input into later calculations, which

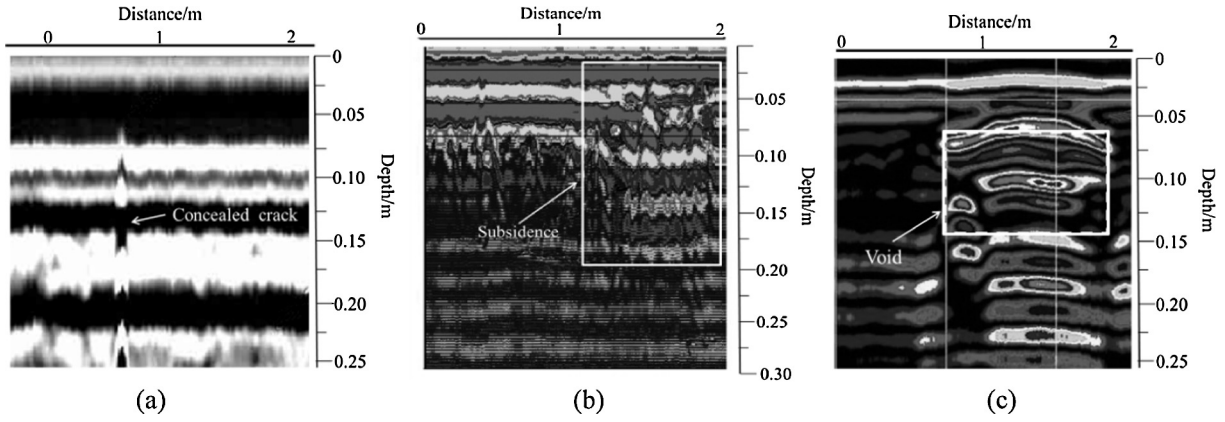

Fig. 4. GPR images of typical highway damage.

Table 1
Quantity of different types of damage in GRP images.

	Concealed crack	Subgrade settlement	Cavities	No damage
Highway 1	11	12	23	12
Highway 2	34	32	27	21
Highway 3	76	23	32	35
Highway 4	45	16	6	16
Highway 5	34	17	12	18
Total	200	100	100	100

Table 2
Highway structures.

	Surface	Base	Subbase	Roadbed
Highway 1	9 cm AC-13	12 cm ATB-25	24 cm 4% water stability macadam	Soil matrix
Highway 2	9 cm AC-13	18 cm ATB-25	18 cm 2% water stability macadam	Soil matrix
Highway 3	9 cm AC-13C	18 cm ATB-25	18 cm graded crushed stone	Soil matrix
Highway 4	9 cm AC-13C	18 cm ATB-25	18 cm graded crushed stone (Geotechnical pattern room)	Soil matrix
Highway 5	9 cm AC-13C	18 cm ATB-25	18 cm 4% water stability macadam	Soil matrix

Note: AC-13 = Asphalt concrete, 13 is the Max. diameter of particle in aggregates, mm.
ATB-25 = Asphalt-treated base, 25 is the Max. diameter of particle in aggregates, mm.

Table 3
Relative dielectric constants of highway materials.

	AC-13	AC-13C	ATB-25	Graded crushed stone	Water stability macadam
Permittivity	5.11–5.13	5.08–5.29	5.09–5.23	8.58–13.56	9.36–18.76

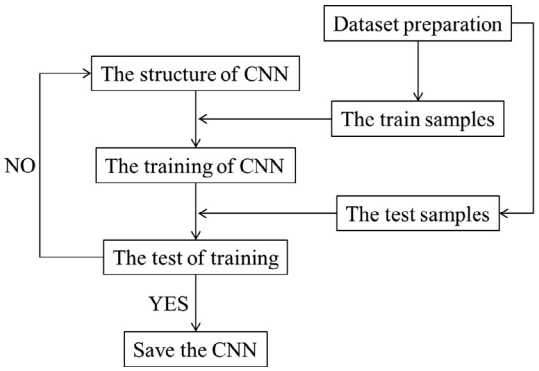

Fig. 5. Process of developing a CNN.

would result in overfitting. The operating principle of S1 and S2 is shown in formula (2). The function $f()$ in formula (2) is calculated in formula (3). Remarkably, down(.) is a pooling function and the max-pooling function was used in this study. Finally, the function of F5 and F6 was to establish a mapping relationship between feature matrices after the pooling function was used and the different types of damage were quadrature encoded.

$$x_j^l = f\left(\sum_{i\subset M_j} x_i^{l-1}\cdot w_{ij}^l + b_j^l\right) \tag{1}$$

$$x_j^l = f(\beta_j^l down(x_j^l) + b_j^l) \tag{2}$$

$$f(x) = sigmoid(x) = \frac{1}{1+e^{-x}} \tag{3}$$

Where:

x_j^l = Feature matrices;
x_j^{l-1} = Image inputs;
w_{ij}^l = Weight of convolution kernels in i line and j row;
b_j^l = Bias of convolution kernels or max-pooling operation;
β_j^l = Multiplicative bias of max-pooling operation;
$f(x)$= Activation function.

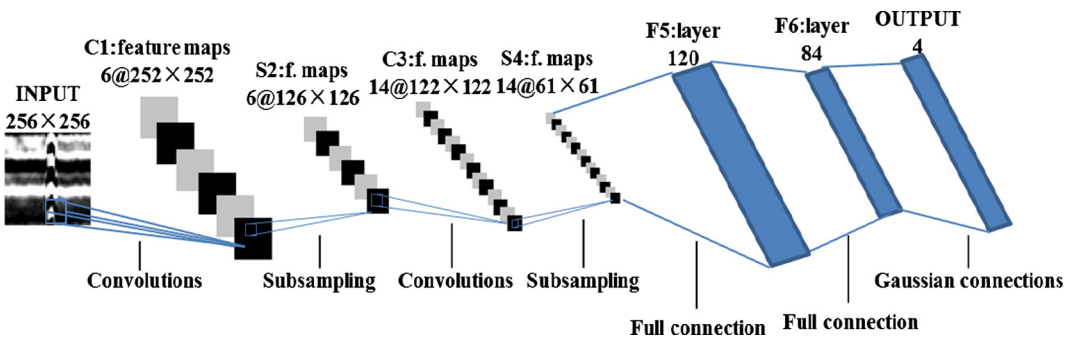

Fig. 6. Structure of the damage recognition CNN.

(c) CNN training

An important property of a CNN is its learning ability. This ability was employed to determine the mapping between input data (2200 images) and target data (the damage types corresponding to images). The mapping was realized by the training of the CNN. The main purpose of the training was to confirm the weights and bias in the CNN. A feed-forward algorithm was used to train the CNN.

The mechanism of the feed-forward algorithm involves the use of the forward-and-back error propagation theory to decrease the error between the CNN output and the target data [28]. Recognition CNN training using the feed-forward algorithm was designed to decrease the damage type error between the CNN output and the target data. The flowchart that describes the feed-forward algorithm is shown in Fig. 7. The feed-forward algorithm begins by confirming initial random values for weights and biases. After importing 100 randomly selected input images from the training sample, the feed-forward algorithm produced the CNN output. Then, the errors between the target data and the CNN output were calculated. From the error of the feed-forward algorithm in the CNN, the weights and biases were modified by formula (4). The first term is the mean squared error reflecting the gap between output values and target values, while the second is the regularization term used to reduce the range ability of weights and bias to prevent over fitting. The gradient of W and b were calculated using formulas (5) and (6), respectively. In addition, the derivative of the activation function is shown in formula (7).

$$J(W|b) = \left[\frac{1}{m}\sum_{i=1}^{m} J(W|b; x^{(i)}|y^{(i)})\right] + \frac{\varepsilon}{2}\sum_{l=1}^{nl+1}\sum_{i=1}^{Sl+1}\sum_{j=1}^{Sl+1}(W_{ji}^{l})^2 \tag{4}$$

$$W_{ij}^{(l)} = W_{ij}^{(l)} - \alpha\frac{\partial}{\partial W_{ij}^{(l)}}J(W,b) \tag{5}$$

$$b_{i}^{(l)} = b_{i}^{(l)} - \alpha\frac{\partial}{\partial b_{ij}^{(l)}}J(W,b) \tag{6}$$

$$f'(x) = Sigmoid\prime(x) = \frac{e^{-x}}{(1+e^{-x})^2} \tag{7}$$

where

W and b represent the weights and biases of the CNN, respectively.
$(x(m), y(m))$ = Greyscale images;
ε = Tradeoff control parameter.

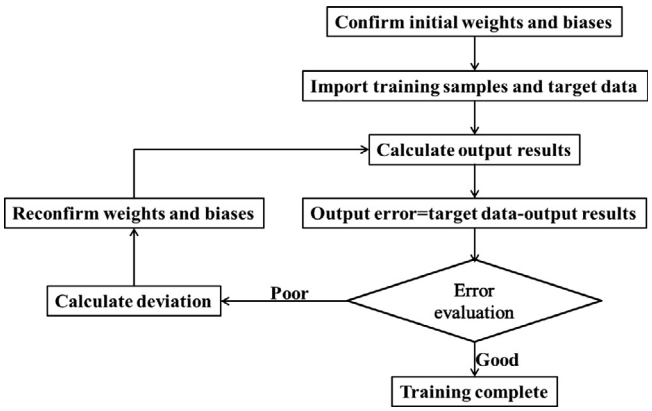

Fig. 7. Flow chart of feed-forward algorithm.

Each process described above was a named iteration. After each iteration is completed, 100 images were imported to the CNN again to evaluate the last iteration. The accuracy rate was used to evaluate each iteration. Based on highway performance assessment standards (JTG H20-2007) [19] and our experience, the training was considered complete if the accuracy rate was more than 0.95 and stable. Correspondingly, the next iteration should be made on the CNN if these requirements are not met.

(d) CNN test

In the training, the accuracy rate satisfying the requirements implied that the recognition CNN produced a good output for the training samples. However, it was not sure whether the CNN has a precise recognition capacity. Therefore, the rest of the 6842 images were imported into the CNN for testing. The result of testing was evaluated by mean squared error (MSE) using formula (8). The recognition CNN had a precise recognition capacity if the accuracy rate was greater than 0.95.

$$MSA = \frac{1}{n}\sum_{i=1}^{n}(target - predicted)^2 \tag{8}$$

All images with concealed cracks were used as a dataset for the location and feature extraction CNNs.

3.1.2. Performance of recognition

The results of each iteration are shown in Fig. 8. The results of iterations were evaluated by the error rate of classification. The horizontal axis represents the number of the iteration. The total number of iterations needed to train the recognition CNN was 30. The vertical axis represents the error rate of the CNN. Predictably, the accuracy rate improved from 0.09 to 0.998. Meanwhile, the accuracy rate was 0.981, in response to the request after the 14th iteration. In order to avoid the influence of individual differences, the number of iterations was prolonged until the accuracy rate was stable. As shown in Fig. 8, the accuracy rate was stable during the 15th–30th iterations, which met all requirements. The result indicated that the recognition CNN distinguished concealed cracks from other damage in 2200 GPR images with no error. After training, the testing sample was imported to the CNN and found no error in recognition. Therefore, the CNN has a precise recognition capacity for concealed cracks. Then, all images with concealed cracks were used as a dataset for the location CNN and the feature extraction CNN.

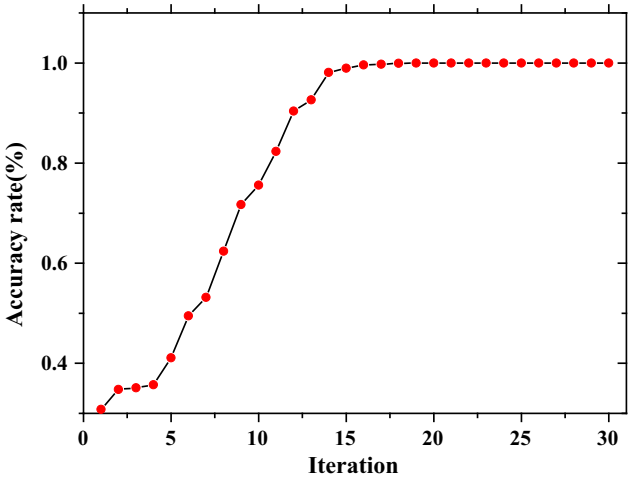

Fig. 8. Damage recognition accuracy rate.

3.2. Location CNN

3.2.1. Design approach for the location CNN

Convolutional neural networks are also used for local pedestrians and traffic signs in images [29–31]. This property can be expanded to local concealed cracks in GPR images and in turn, measure their length by calculating the length of the EdgeBox as shown in Fig. 9. The development of the location CNN is described by the steps shown in Fig. 9.

(a) Preparation of training samples and test samples

A labeled database was needed to complete training and testing for location CNN. 2256 concealed crack images identified by the recognition CNN were divided into 5233 64 × 64 images. As shown in similar location studies on pedestrians, traffic signs, and slab information [30–32], the typical sizes of training and testing samples for locating were in the range of approximately 2000–20,000 images. Values within this range of typical sizes were used in our research on location. 4000 64 × 64 images were selected from 5233 images to manually label with the locations for concealed cracks. These images were to be used as training samples. Because the GPR images were numbered based on stake marks in a lane by the LTD system, we located the cracks simply by locating cracks in the GPR images. To locate concealed cracks, we designed edged boxes as shown in Fig. 9, whose top edges were coincident with the tops of concealed cracks and whose lateral margins were coincident with the sides of concealed cracks at the bottom of the 64 × 64 images. Regarding the difficulty associated with determining crack lengths using core samples in a certain position, the lengths of concealed cracks were calculated based on GPR images and origination points in sub-bases. For the vertical resolution of the 500 MHz antenna (0.15–0.27 cm) to meet the requirement of detecting the crack geometry [19], lengths of cracks in surfaces were acquired from GPR images. Because the origination points are located in the sub-bases, the lengths of cracks in bases and sub-bases were equal to the thicknesses of the bases and sub-bases. Therefore, the total lengths of the cracks could be calculated by adding the lengths of the cracks in the surfaces, bases, and sub-bases. So, 4000 labeled images were used as the training samples, and the rest of the 5233 images were used as test samples. Because all of the images were created by the LTD-2000 GPR and the 500 MHz shielding antenna, the concealed crack length in images has a fixed ratio to their actual length.

(b) CNN structure

The location CNN had a similar structure to the recognition CNN. It was composed of two convolutional layers (C1 and C2) and two subsampling layers (S1 and C2), followed by two full connection layers (F1 and F2) and the output layer. The details of the CNN are shown in Fig. 10. The size of input layer was 64 × 64. Because the size of input layer was equal to the sizes of the images, it was selected based on the two principles mentioned earlier. Similar CNNs used for locating pedestrians, traffic signs, and slab information [30–32] were referred to, and these references utilized images sizes that were in the range of 32 × 32–128 × 128. Considering the two principles and similar CNNs for location, 64 × 64 was selected as the image size for the location.

(c) CNN training

The feed-forward algorithm mentioned in Section 3.1.1 was also used to train the location CNN. However, the training had two goals, as shown in Fig. 8: measurement of crack location and length recognition. The errors in crack location and length recognition were calculated. The crack location errors were measured as the deviation in the coordinates of the edge box between the CNN output and the labeled box edge. The crack length errors showed a long deviation between the CNN output and the actual length. The deviations of the location and length measurement CNN were evaluated by MSE. MSE was calculated using formula (8). Based on the highway performance assessment standards (JTG H20-2007) [19] and our experience, the training was considered completed when the MSE was less than 0.95 and stable. Correspondingly, the next iteration was to be made in case the CNN did not satisfy the requirement. The rest of the process was the same as that used for the recognition CNN.

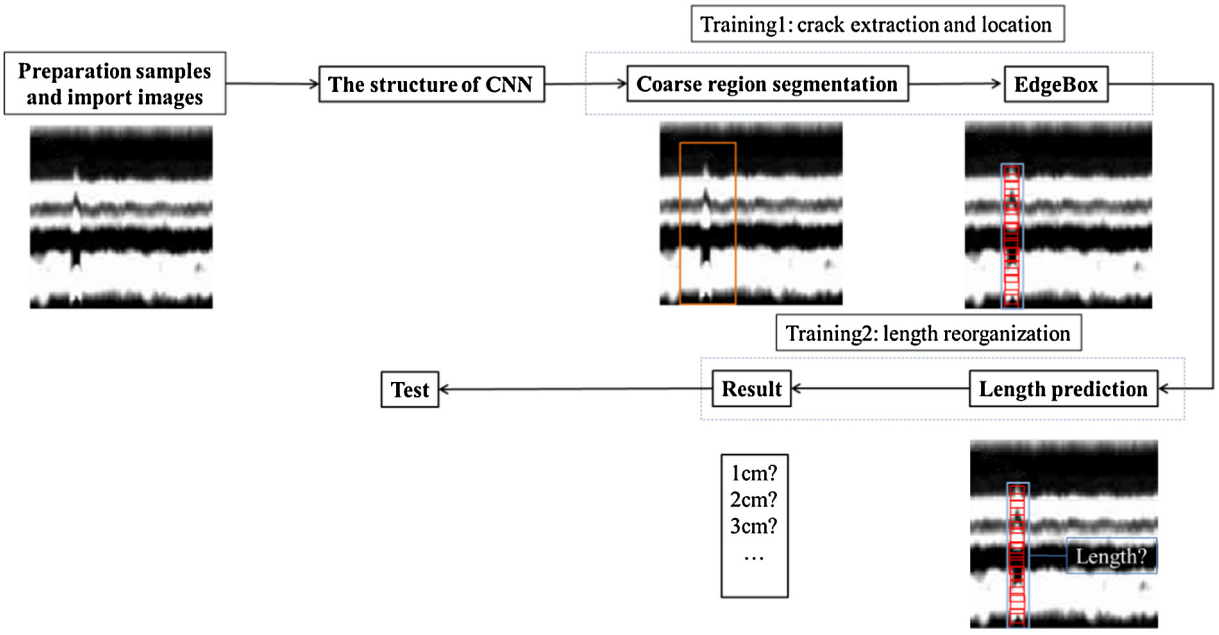

Fig. 9. Pipeline of the proposed method.

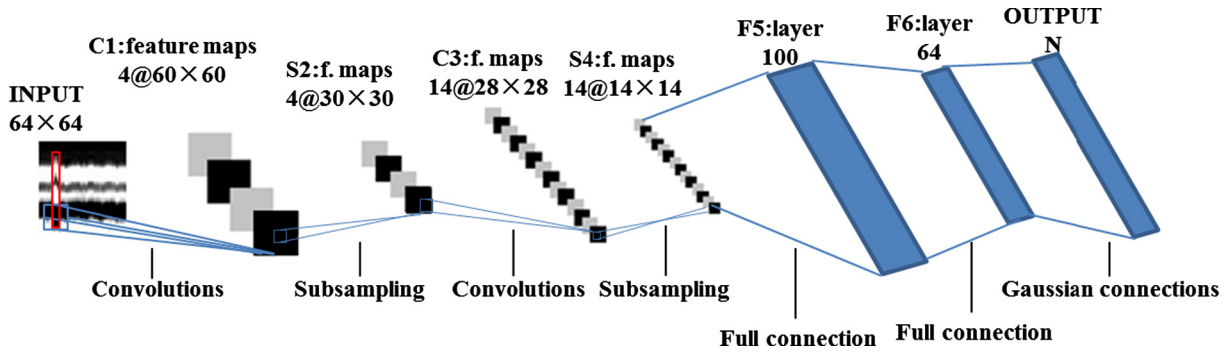

Fig. 10. Structure of the location and length recognition CNN.

(d) CNN test

The previously mentioned test samples were used to test the location and length measurement capability of the CNN after training was completed. All 5233 cracks images were used as the dataset for the feature extraction CNN in the follow-up work.

3.2.2. Performance of the location CNN

The location CNN was trained using the labeled dataset. It was evaluated by the MSE of the edge box coordinates and the concealed crack length. Fig. 11a shows part of the results of the locations in three concealed crack images. Fig. 11b shows the MSE of the location CNN. The broken dotted line is the MSE of the edge box coordinates and the broken line with squares is the MSE of the length. The result indicated that the CNN located concealed cracks correctly and recognized the length of concealed cracks with a 0.2543 cm MSE. Notably, after the 120th iteration, the two MSEs were stable.

Then, the previously mentioned test samples were used to test the location and length measurement capability of the CNN after training was completed. The rest of the 5233 crack images were used as test samples for this testing. The MSE of the edge box and length was 0.327 cm and 0.732 cm, respectively. The maximum length error in the test samples was 0.978 cm, and the average length error was 0.504 cm, which met the requirement for highway engineering detection. Finally, all 5233 cracks images located were used as a dataset for the feature extraction CNN.

3.3. Feature extraction CNN

3.3.1. Design approach for the feature extraction CNN

A large amount of information on damage features is desired for highway maintenance. To acquire additional information on concealed cracks, an attempt was made to extract crack features from GPR images of concealed cracks. The CNN is widely used to extract facial features [33–37]. This capability can be extended to extract

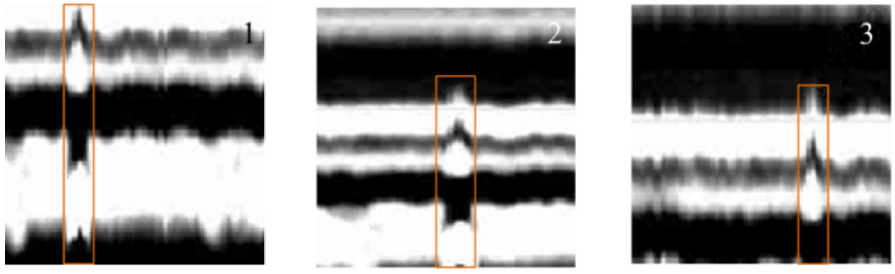

(a)

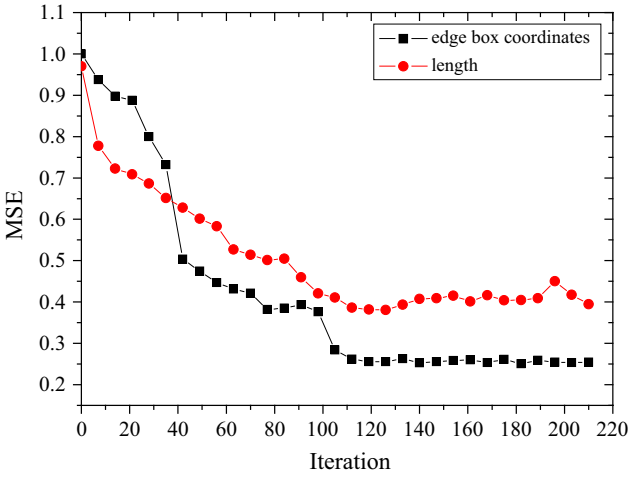

(b)

Fig. 11. Results of location and length recognition.

feature points in GPR concealed crack images, and these feature points can be used for 3D reconstruction. Therefore, a feature extraction CNN was designed to perform this work. The development of the feature extraction CNN is described by the following steps.

(a) Preparation of training samples and test samples

Another labeled dataset was required to complete this process. As shown in similar feature exaction studies on abnormal behavior detection and facial feature detection [29,38], typical training and

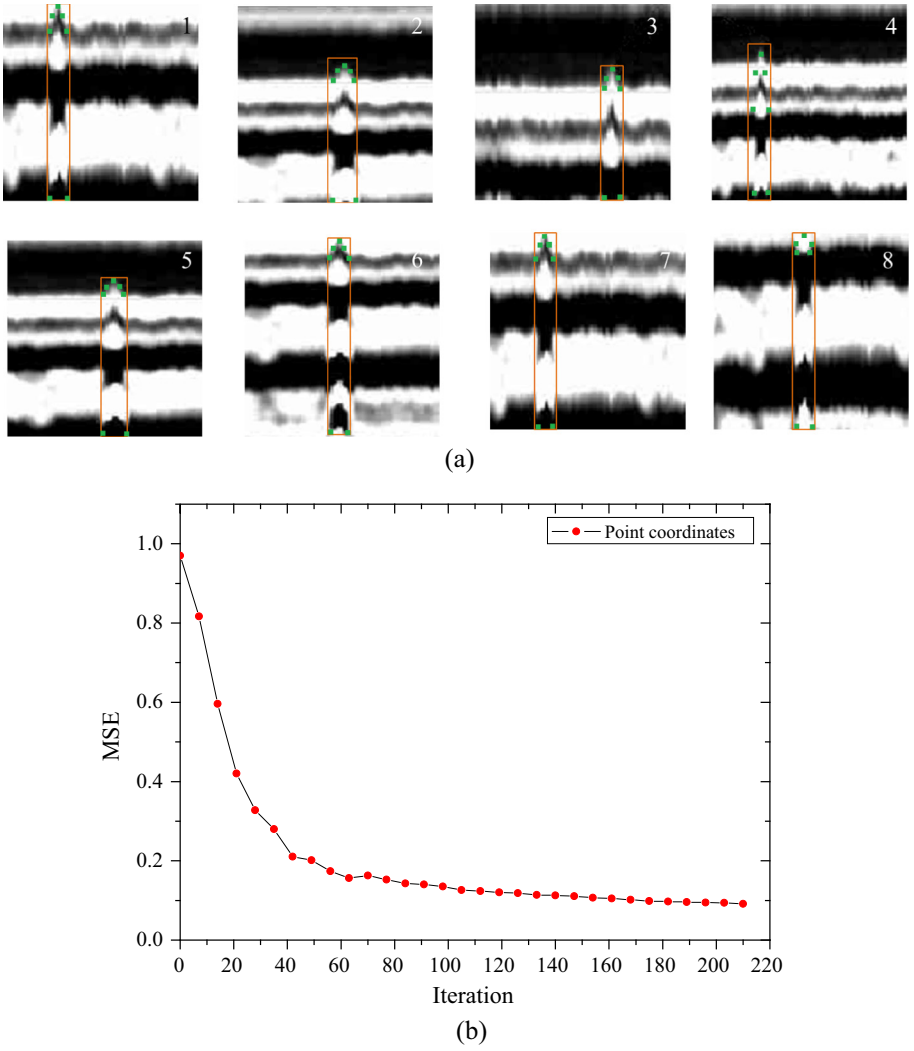

Fig. 12. Results of feature point extraction.

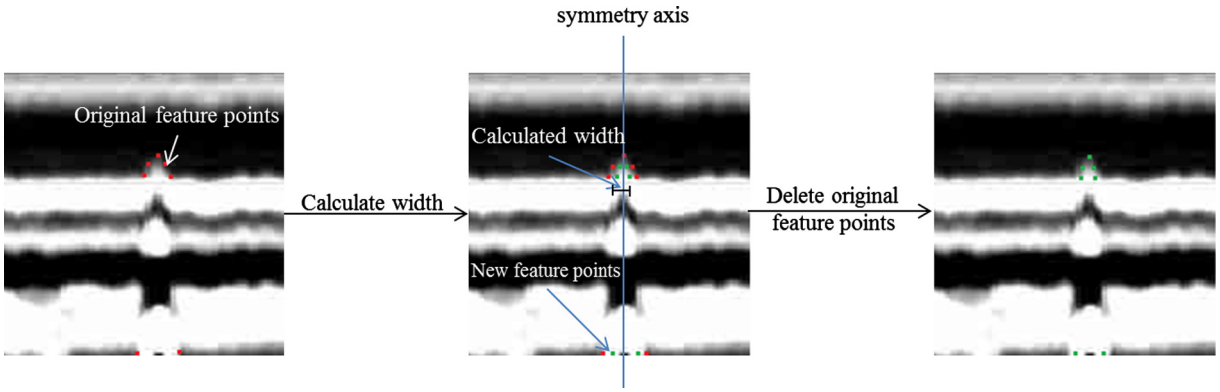

Fig. 13. Process of changing x-coordinates.

testing sample sizes for exacting features were in the range of approximately 2000–20,000 images. Values within this range of typical sizes were used in our research on feature exaction. All 5233 64 × 64 images with located concealed cracks were acquired by the location CNN. Four thousand images were selected randomly to manually label different geometric feature points. Therefore, these 4000 labeled images were used as the training samples, and the rest of the unlabeled images were used as test samples.

(b) CNN structure

The feature extraction CNN had the same structure as the location CNN, but the number of output neurons was seven, which represented seven shape coordinates for feature points.

(c) CNN training

The feed-forward algorithm mentioned in Section 3.1.1 was also used to train the feature extraction CNN. However, this time the training was to designed to extract sharpness features. Errors in feature extraction were recognized as coordinate deviations between the CNN output and the labeled feature points. The rest of the training process was the same as that for the recognition CNN.

(d) CNN test

The deviations in the feature extraction CNN were evaluated by MSE. MSE was calculated by using formula (4). The previously mentioned test samples were used to test the feature extraction capability of the CNN after each iteration was completed.

3.3.2. Performance of the feature extraction CNN

The feature extraction CNN was trained by the labeled dataset. It was evaluated by the MSE of the coordinates deviation between the CNN output and the labeled feature points. Fig. 11a shows the results of feature extraction in eight concealed crack images. Fig. 12b shows the MSE of the CNN. The horizontal axis represents

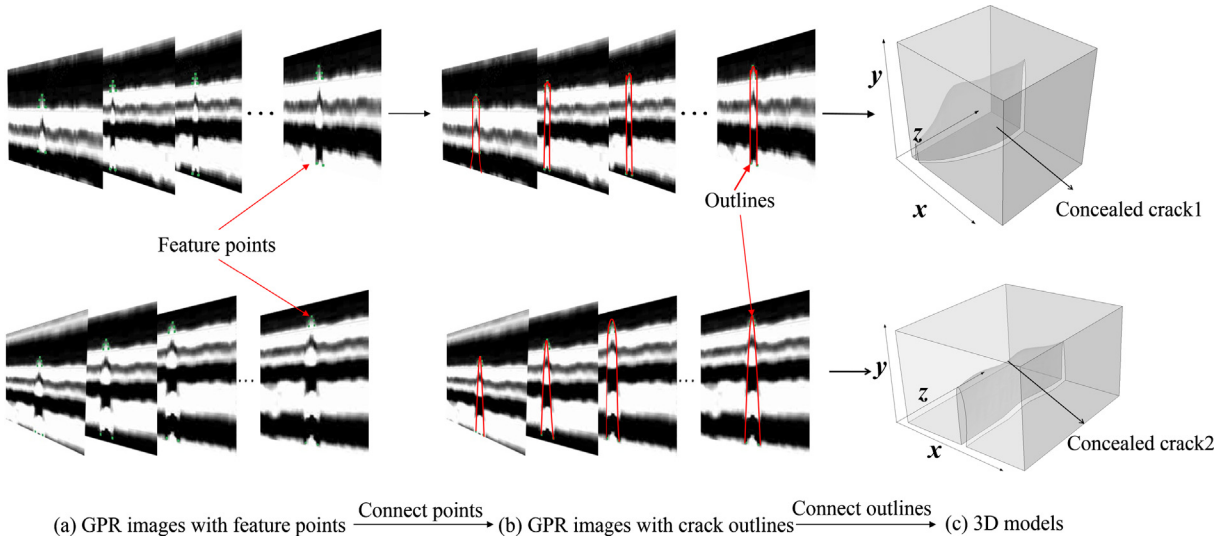

Fig. 14. Process of 3D reconstruction.

Table 4
Road structures.

Roads			Highway 1	Highway 2	Highway 3	Highway 4
Road structures	Surfaces	Upper layers	4 cm SBS Modified Asphalt Concrete (AC-16C)	5 cm Asphalt Concrete (AC-16C)	4 cm Asphalt Concrete (AC-16C)	4 cm Stone mastic asphalt (SMA-13)
		Middle layers	7 cm SBS Modified Asphalt Concrete (AC-20C)	6 cm Asphalt Concrete (AC-20C)	6 cm Asphalt Concrete (AC-20C)	7 cm SBS Modified Asphalt Concrete (AC-20C)
		Lower layers	8 cm Asphalt Concrete (AC-25C)	8 cm Bituminous Stabilized Macadam (ATB-30C)	9 cm Asphalt Concrete (AC-25C)	8 cm Asphalt Concrete (AC-25C)
	Seal coats		Modified asphalt synchronized crushed stone seal layers			
	Bases	Upper bases	8 cm Bituminous Stabilized Macadam (ATB-30C)	32 cm Cement stabilized gavels	32 cm Cement stabilized gavels	41 (42) cm Cement stabilized gavels
		Lower bases	40 cm Cement stabilized gavels			
	Sub-bases		24 (25) cm Natural gravel	20 cm Cement stabilized natural gavels	20 cm Cement stabilized natural gavels	22 (24) cm Cement stabilized natural gavels

Note: AC-13 = Asphalt concrete, 13 is the Max. diameter of particale in aggregates, mm.
ATB-25 = Asphalt-treated base, 25 is the Max. diameter of particale in aggregates, mm.
SMA-13 = Stone mastic asphalt, 13 is the Max. diameter of particale in aggregates, mm.

the number of the iteration, and the vertical axis represents the MSE of the CNN for the corresponding iteration. The result indicated that this CNN extracted feature points correctly, which met the demand for highway engineering detection.

3.3.3. Design approach for 3D reconstruction

To realize 3D reconstruction of concealed cracks, the crack widths need to be measured. However, because the crack widths are smaller than half of the first Fresnel zone diameter, they cannot be measured by GPR directly [6,39]. Therefore, the width distance between feature points is not the real width of the crack. Guo et al. [40] found that there was an approximate linear relationship between the crack widths and the scattering wave at the top of crack. Therefore, the x-coordinates of the feature points were modified based on formula (9). The process of modification is shown in Fig. 13. Then, 3D reconstruction is realized based on the new coordinates of the feature points, as shown in Fig. 14. Based on the points in each image, an outline of a crack was drawn. Then, these outlines were smoothly superimposed into the sequence of pavement stake marks. All of the details of concealed crack can be seen

Table 5
Relative dielectric constants of highway materials.

Structures	Types of highway materials				
Surfaces	AC-16C	AC-20C	AC-25C	ATB-30C	SMA-13
	5.04–5.23	4.96–5.25	4.78–5.16	4.87–5.12	5.17–5.21
Bases	ATB-30C	Cement stabilized gavels		Cement stabilized natural gavels	
	4.85–4.98	8.92–14.37		8.65–15.12	

Table 6
Confusion matrix.

	0–2 cm	2–4 cm	4–6 cm	6–8 cm	8–10 cm	10–12 cm	12–14 cm	14–16 cm
0–2 cm	69							
2–4 cm	2	15	1					
4–6 cm		1	23	2				
6–8 cm			3	43	3			
8–10 cm				2	54			
10–12 cm					4	15	3	
12–14 cm						1	54	1
14–16 cm							2	38
Total	71	16	27	47	61	16	59	39
Error	2	1	4	4	7	1	2	1

Note: Row heading stands for crack lengths in actual measurement.
column heading stands for crack lengths in CNN calculation.

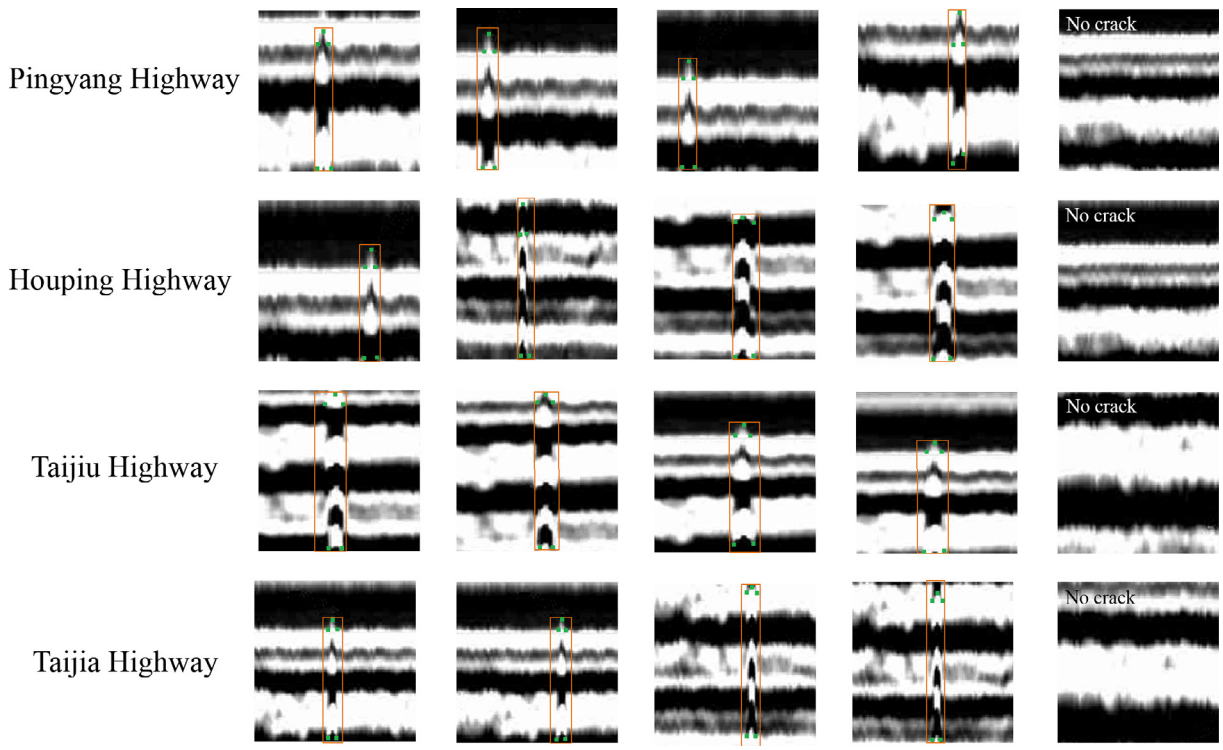

Fig. 15. Results of road detection.

Table 7
Quantity of different crack images.

	Crack1	Crack2	Crack3	Crack4	Crack5	Crack6	Crack7	Crack8	Crack9	Crack10
Volume/cm^3	1027.40	681.8	235.76	345.75	532.46	236.24	367.89	523.45	410.02	108.97
Roads	Highway1	Highway1	Highway1	Highway2	Highway3	Highway3	Highway3	Highway4	Highway4	Highway4

in the 3D model; for instance, the volume was acquired. The volumes of these two cracks were based on 3D models. The results were 1027.40 cm^3 and 681.8 cm^3. A more advanced CNN should be developed in future work to obtain a greater number of points to describe the concealed cracks in greater detail.

$$E_z = 1200x \tag{9}$$

where

E_z = Peak value of electric field intensity at the top of crack, mV/mm;
x = Crack width, mm.

4. Application in pavement

All three CNNs were used to measure concealed cracks in practice after the processes mentioned in Section 3. Four highways in Shanxi, China were observed. Fifty images from each road were acquired by following the above-mentioned collection method, and the total number of GPR images was 200. The highway structures and relative dielectric constants of the highway materials are listed in Table 4 and Table 5, respectively. First, 200 images were transformed into grey-scale maps and divided into 256 × 256 pixel images. Second, 3200 256 × 256 pixel grey-scale maps were imported into the recognition CNN and classified based on the types of distress. Third, greyscale maps with concealed cracks were inserted into the location CNN and the feature extraction CNN. Finally, the results from the location CNN and the feature extraction CNN were used to locate and rebuild concealed cracks.

The detection results showed that the recognition CNN can distinguish concealed cracks from other types of damage with zero error. Eighty-two images with concealed cracks were acquired and divided into 336 64 × 64 pixel images. All 64 × 64 pixel images were imported into the location CNN and the feature extraction CNN. The calculation results for the location CNN are presented in Table 6. It can be seen from the table that the maximum length error was less than 1 cm and the average length error was 0.587 cm. The representative results of location and feature extraction are shown in Fig. 15. Finally, 10 cracks were selected to calculate volume, and the results are shown in Tab.7. All of the results showed that the CNN system met the demand for highway engineering detection.

From the results obtained from the three CNNs for concealed cracks, several suggestions could be made regarding the maintenance of the four highways. For example, detection efficiency could be improved by saving time when classifying the types of distresses in GPR images by using the recognition CNN. In addition, predictions for when concealed cracks would change to reflection cracks could be made based on the length of the concealed cracks. The filler volumes for grouting the 10 cracks could be calculated based on crack volumes shown in Table 7.

5. Conclusions

In this study, the application of CNN for the automatic recognition, location, length measurement, and 3D reconstruction of concealed cracks (in batches) using GPR images was performed. The following conclusions can be drawn from the results.

1) The recognition CNN was designed to distinguish concealed cracks from other pavement damage in GPR radar images. In testing, it demonstrated the ability to distinguish concealed cracks from other pavement damage in 6842 GPR images with no error.
2) The location CNN located and measured the length of concealed cracks in images obtained from the results generated by the recognition CNN. The CNN can recognize concealed cracks with a 0.2543 MSE. The maximum length error in 5233 test samples was 0.978 cm, and the average length error was 0.504 cm. Both measuring errors satisfied the demand for highway engineering detection.
3) The feature point extraction CNN was used to extract crack shape properties for 3D reconstruction. However, the output of coordinates cannot be directly used in 3D reconstruction. A change in width coordinates should be conducted based on an empirical formula.
4) A more accurate formula should be developed to obtain more accurate width coordinates. In addition, a more advanced feature point extraction method should be developed to obtain a greater number of points, from which the concealed cracks can be described in greater detail.
5) A more advanced CNN should be developed to obtain a greater number of points to describe the concealed cracks in greater detail. This should be the focus of future work.
6) Some suggestions about highway maintenance could be made based on the results obtained from the three CNNs, such as crack growth trends and filler volumes for grouting.

Acknowledgments

The authors deeply appreciate the support from the Northeast Forestry University and the foundations for the project of Heilongjiang Traffic and Transportation Department, and the National and Local Joint Engineering Materials Laboratory of Traffic Engineering and Civil Engineering, Chongqing Jiaotong University (No: LHSYS-2016-002).

References

[1] A.P. Annan, N. Diamanti, J.D. Redman, S.R. Jackson, Ground-penetrating radar for assessing winter roads, Geophysics 81 (1) (2016) A101–A109.
[2] Dar-Hao Chen, Feng Hong, Wujun Zhou, Peng Ying, Estimating the hotmix asphalt air voids from ground penetrating radar, NDT and E Int. 68 (2014) 120–127.
[3] Hai Liu, Motoyuki Sato, in situ measurement of pavement thickness and dielectric permittivity by GPR using an antenna array, NDT and E Int. 64 (2014) 65–71.
[4] Zhao Shan, Imad L. Al-Qadi, Development of an analytic approach utilizing the extended common midpoint method to estimate asphalt pavement thickness with 3-D ground penetrating radar, NDT and E Int. 78 (2016) 29–36.
[5] M. Solla, S. Lagüela, H. González-Jorge, P. Arias, Approach to identify cracking in asphalt pavement using GPR and infrared thermography methods: preliminary findings, NDT and E Int. 62 (2014) 55–65.
[6] L.U. Cheng-Ming, Q.I.N. Zhen, Z.H.U. Hai-Long, L.I. Xiu-Zhong, Practical methods for detection of concealed cracks in highway pavement using ground penetration radar data, Chin. J. Geophys. 50 (5) (2007) 1558–1568 (in Chinese).
[7] Xu Xingxin, Zeng Qiaosong, Li Dong, Wu Jin, Wu Xiangan, Shen Jinyin, GPR detection of several common subsurface voids inside dikes and dams, Eng. Geol. 111 (1–4) (2010) 31–42.
[8] V. Pérez-Gracia, F. García García, Abad I. Rodriguez, GPR evaluation of the damage found in the reinforced concrete base of a block of flats: A case study, NDT and E Int. 41 (5) (2008) 341–353.

[9] P. Szymczyk, M. Szymczyk, Non-destructive building investigation through analysis of GPR signal by S-transform, Autom. Constr. 55 (2015) 35–46.
[10] Cécile Barat, Christophe Ducottet, String representations and distances in deep convolutional neural networks for image classification, Pattern Recogn. 54 (2016) 104–115.
[11] Baoguang Shi, Xiang Bai, Cong Yao, Script identification in the wild via discriminative convolutional neural network, Pattern Recogn. 52 (2016) 448–458.
[12] Biao Leng, Shuang Guo, Xiangyang Zhang, Zhang Xiong, 3D object retrieval with stacked local convolutional autoencoder, Sig. Process. 112 (2015) 119–128.
[13] Xu Jun, Xiaofei Luo, Guanhao Wang, Hannah Gilmore, Anant Madabhushi, A deep convolutional neural network for segmenting and classifying epithelial and stromal regions in histopathological images, Neurocomputing 191 (2016) 214–223.
[14] Xu Tiantian, Fan Zhu, Edward K. Wong, Yi. Fang, Dual many-to-one-encoder-based transfer learning for cross-dataset human action recognition, Image Vis. Comput. 55 (2) (2016) 127–137.
[15] E.P. Ijjina, K.M. Chalavadi, Human action recognition using genetic algorithms and convolutional neural networks, Pattern Recogn. 59 (2016) 199–212.
[16] J. Arevalo, F.A. González, R. Ramos-Pollán, J.L. Oliveira, M.A. Guevara Lopez, Representation learning for mammography mass lesion classification with convolutional neural networks, Comput. Methods Programs Biomed. 127 (2016) 248–257.
[17] Q. Li, Z. Jin, C. Wang, D.D. Zeng, Mining opinion summarizations using convolutional neural networks in Chinese microblogging systems, Knowl.-Based Syst. 107 (2016) 289–300.
[18] Zishun Liu, Juyong Zhang, L. Liu, L. Liu Ligang Liu, Upright orientation of 3D shapes with convolutional networks, Graph. Models 85 (5) (2016) 22–29.
[19] JTG H20–2007, Highway Performance Assessment Standards, Beijing, China.
[20] Huiming Fang, Hui Luo, Hongping Zhu, The feasibility of continuous construction of the base and asphalt layers of asphalt pavement to solve the problem of reflective cracks, Constr. Build. Mater. 119 (2016) 80–88.
[21] Shihui Shen, Weiguang Zhang, Lin Shen, Hai Huang, A statistical based framework for predicting field cracking performance of asphalt pavements: Application to top-down cracking prediction, Constr. Build. Mater. 116 (2016) 226–234.
[22] Rui Li, Jiaqi Chen, Tianshu Zhou, Jianzhong Pei, Preparation and characterization of novel light induced self-healing materials for cracks in asphalt pavements, Constr. Build. Mater. 105 (2016) 336–342.
[23] Hu Yaocong, Huan Chang, Fudong Nian, Yan Wang, Teng Li, Dense crowd counting from still images with convolutional neural networks, J. Visual Commun. Image Represent. 38 (2016) 530–539.
[24] Fudong Nian, Teng Li, Yan Wang, Xu Mingliang, Wu Jun, Pornographic image detection utilizing deep convolutional neural networks, Neurocomputing 210 (2016) 283–293.
[25] Yi Sun, Xiaogang Wang, Xiaoou Tang. Deep Convolutional Network Cascade for Facial Point Detection. IEEE Conference on Computer Vision and Pattern Recognition, 2013.
[26] Iveta Mrazova, Marek Kukacka, Can deep neural networks discover meaningful pattern features?, Procedia Comput Sci. 12 (2012) 194–199.
[27] Evgeny A. Smirnov, Denis M. Timoshenko, Serge N. Andrianov, Comparison of regularization methods for imagenet classification with deep convolutional neural networks, AASRI Procedia 6 (2014) 89–94.
[28] Adriana Trocoli Abdon Dantas, Monica Batista Leite, Koji De Jesus Nagahama, Prediction of compressive strength of concrete containing construction and demolition waste using artificial neural networks, Constr. Build. Mater. 38 (2013) 717–722.
[29] S. Zhou, W. Shen, D. Zeng, M. Fang, Y. Wei, Z. Zhang, Spatial–temporal convolutional neural networks for anomaly detection and localization in crowded scenes, Sig. Process. Image Commun. 47 (2016) 358–368.
[30] Y. Hu, H. Chang, F. Nian, Y. Wang, T. Li, Dense crowd counting from still images with convolutional neural networks, J. Vis. Commun. Image Represent. 38 (2016) 530–539.
[31] Y. Zhu, C. Zhang, D. Zhou, X. Wang, X. Bai, W. Liu, Traffic sign detection and recognition using fully convolutional network guided proposals, Neurocomputing. 19 (2016) 758–766.
[32] Sang Jun Lee, Sang Woo Kim, Localization of the slab information in factory scenes using deep convolutional neural networks, Expert Syst. Appl. 77 (2017) 34–43.
[33] E.P. Ijjina, K.M. Chalavadi, Human action recognition using genetic algorithms and convolutional neural networks, Pattern Recogn. 59 (2016) 199–212.
[34] Yuan Dong, Yinan Liu, Shiguo Lian, Automatic age estimation based on deep learning algorithm, Neurocomputing. 187 (2016) 4–10.
[35] Mohammadreza Ebrahimi, Ching Y. Suen, Olga Ormandjieva, Detecting predatory conversations in social media by deep Convolutional Neural Networks, Digital Invest. 18 (2016) 33–49.
[36] Y. Dong, Y. Wu, Adaptive cascade deep convolutional neural networks for face alignment, Comput. Stand. Interfaces 42 (2015) 105–112.
[37] Feng Litong, Po Lai-Man, Xu Li Yuming, Yuan Fang Xuyuan, Cheung Terence Chun-Ho, Cheung Kwok-Wai, Integration of image quality and motion cues for face anti-spoofing: a neural network approach, J. Vis. Commun. Image Represent. 38 (2016) 451–460.
[38] Dong Wang, Jing Yang, Jiankang Deng, Qingshan Liu, FaceHunter: a multi-task convolutional neural network based face detector, Sig. Process. Image Commun. 47 (2016) 476–481.
[39] X. Xu, Q. Zeng, D. Li, J. Wu, X. Wu, J. Shen, GPR detection of several common subsurface voids inside dikes and dams, Eng. Geol. 111 (1–4) (2010) 31–42.
[40] G.U.O. Shili, Z.H.U. Peimin, S.H.I. Xinghua, L.I. Xiuzhong, Comparative analysis on response of gound penetrating radar wave field to crack width, Chin. J. Radio Sci. 28 (1) (2013) 130–136 (in Chinese).